Appl Magn Reson (2011) 40:471–479
DOI 10.1007/s00723-011-0213-9

Applied
Magnetic Resonance

Magnetic Properties of Monomer and Dimer Tetrahedral VO_x Entities Dispersed on Amorphous Silica-based Materials: Prediction of EPR Parameters from Relativistic DFT Calculations and Broken Symmetry Approach to Exchange Couplings

Piotr Pietrzyk · Zbigniew Sojka

Received: 28 November 2010 / Revised: 21 February 2011 / Published online: 25 March 2011

Abstract Molecular structures of the isolated tetrahedral oxovanadium(IV) and bridged μ-oxo-divanadium(IV) complexes hosted by the clusters mimicking surfaces of amorphous silica-based materials were investigated using density functional theory (DFT) calculations. Principal values of the **g** and **A** tensors for the monomer vanadyl species were obtained using the coupled-perturbed DFT level of theory and the spin–orbit mean-field approximation (SOMF). Magnetic exchange interaction for the μ-oxo bridged vanadium(IV) dimer was investigated within the broken symmetry approach. An antiferromagnetic coupling of the individual magnetic moments of the vanadium(IV) centers in the $[VO–O–VO]^{2+}$ bridges was revealed and discussed in detail. The coupling explains pronounced decrease of the electron paramagnetic resonance signal (EPR) intensity, observed for the reduced VO_x/SiO_2 samples with the increasing coverage of vanadia, in terms of transformation of the paramagnetic monomer species into the dimers with $S = 0$ ground state.

1 Introduction

Spectroscopic and chemical properties of the supported oxide catalysts are featured by their pronounced surface area and the presence of the structural and morphological defects. The resultant inherent heterogeneity of the surface sites gives rise to low-symmetry phenomena in the electron paramagnetic resonance (EPR) spectra and apparent speciation of the paramagnetic surface species [1]. As a consequence, a great deal of significant chemical information about the investigated system can only be recovered with the help of computer simulation of the

This work was originally presented during the Asia–Pacific ESR/EPR Symposium 2010.

P. Pietrzyk (✉) · Z. Sojka
Faculty of Chemistry, Jagiellonian University, ul. Ingardena 3, 30-060 Krakow, Poland
e-mail: pietrzyk@chemia.uj.edu.pl

experimental spectra [2], supported by quantum chemical calculations of the EPR parameters (**g, A** and **D** tensors, exchange coupling constants *J*) [3, 4]. In such an approach, the experiment provides solid constraints for validation of the computational scheme, while theory allows for an in-depth molecular interpretation of the spin-Hamiltonian parameters and their structure sensitivity [5].

In the present study, a model catalytic system composed of the VO_x entities dispersed on the surfaces of amorphous silica such as vitreous SiO_2 or mesoporous MCM-41, MCM-48, SBA-15 was investigated. Such materials have been found as a catalytically active system in, e.g., oxidative dehydrogenation [6] or selective oxidation of hydrocarbons [7]. It has been found that the activity of VO_x/SiO_2 depends on the ratio of the monomeric vanadyl species V=O to the polymeric entities characterized by the V–O–V linkages [8]. The monomeric species containing terminal V=O groups are predominantly formed at low vanadium loadings, while at higher coverage these species transform into the polyvanadates. However, the nature of the active vanadium ensembles in the selective oxidation and oxidative dehydrogenation is still a matter of debate. The presence of agglomerated surface vanadium not only has a direct impact on the catalyst selectivity but also may deteriorate activity, since not all of the vanadium atoms are accessible to the reactant molecules. Thus, in order to increase the number of the isolated vanadium species, the high-surface-area supports such as the already mentioned MCM-41, MCM-48, SBA-15 are frequently used [9, 10].

In the reaction conditions, the surface-isolated and polynuclear vanadium sites are engaged in the V^V/V^{IV} redox cycles that can be easily followed with EPR technique, even in the operando conditions [11, 12]. Whereas the mononuclear vanadium(IV) has been already characterized both experimentally and theoretically [3, 6, 7, 11–15], information about electronic and magnetic structure of the polynuclear vanadium(IV) entities is rather scarce [16]. A μ-oxo-divanadium(IV) V^{IV}–O–V^{IV} dimer has been considered as a good model of such species in accounting for the mechanism of the oxidative dehydrogenation of propane [11].

The aim of this work was to propose the molecular models for reduced forms of the isolated and dimer vanadyl species supported on surfaces composed of amorphous silica, and to ascertain their magnetic structure in terms of spin-Hamiltonian parameters (quantification of the **g** and hyperfine **A** tensors, and evaluation of exchange coupling constants *J*).

2 Computational Details

The hosting sites of the silica surface were modeled with the finite clusters cut off from the molecular dynamic model of amorphous SiO_2 [17]. Such surface sites differ in the spatial arrangement of the silanol groups, reflecting variances in the local chemical environment encountered in real systems. The adopted cluster models allow for accommodation of the monomeric or polynuclear surface vanadium complexes [18] and have already been validated in many spectroscopic and computational investigations [14, 18, 19]. In this study, the monomeric vanadyl surface complex was modeled with the $(Si_5O_8H_8)^{2-}(VO^{2+})$ cluster and the dimeric

one with the $(Si_6O_{10}H_{10})^{2-}(VO–O–VO)^{2+}$ epitome. Hereafter, they are referred to as [VO]-**5T** and [VO–O–VO]-**6T**, respectively, according to the nomenclature used in zeolite chemistry, where the size of the ring is denoted by the number of **T** atoms (**T** = Si).

Geometry optimization was performed with the Gaussian03 program (version E.01) [20]. The hybrid Becke, three-parameter, Lee–Yang–Parr (B3LYP) exchange–correlation functional [21, 22] and the all-electron Ahlrichs triple-ζ type (TZV) basis set [23] with one set of the polarization functions were used. The cluster models were fully optimized without any constraints at the spin-unrestricted level, using analytic gradients and the Broyden–Fletcher–Goldfarb–Shanno (BFGS) method [24]. In the case of the dinuclear vanadium(IV) complex, the geometry was optimized in high-spin triplet state, and the stability of the wavefunction was tested.

The spectroscopic parameters (electronic **g** tensor, vanadium hyperfine coupling tensor **A**, and isotropic exchange coupling constants J) were obtained from the single-point calculations, using the clusters with the previously optimized geometries. These calculations were performed with the ORCA package [25], which includes the spin–orbit coupling (SOC), spin-polarization, relativistic mass and diamagnetic gauge corrections. The SOC effects (for **g** and **A** tensors) were treated within the spin–orbit mean-field approximation (SOMF) [26]. The **A** tensor was calculated according to the classical spin-density based formula, including the SOC contribution as a second-order property at the coupled-perturbed Kohn–Sham level of theory [27].

For the dinuclear vanadium(IV) complex, the calculations of the isotropic exchange coupling constant J were based on the broken symmetry approach, originally developed by Noodleman for SCF methods [28] and extended later into density functional theory (DFT) [29]. In this case a well-known phenomenological Hamiltonian of Heisenberg–Dirac–van Vleck was applied:

$$H_{\mathrm{HDvV}} = -2J\hat{S}_1\hat{S}_2, \tag{1}$$

where S_1 and S_2 stand for the total spin angular momenta for two interacting vanadyls. The parameter J is referred to as the magnetic isotropic exchange coupling constant. The convention of the sign is taken in such a way that positive J corresponds to ferromagnetic coupling. The values of the exchange coupling constant were derived from the adiabatic energy differences of the high-spin (HS) and broken-symmetry (BS) states. Having obtained the spin-unrestricted solutions for the determinants corresponding to the maximum spin $S_{\mathrm{HS}} = S_A + S_B$, and broken spin symmetry $S_{\mathrm{BS}} = |S_A - S_B|$, the J values were calculated using the Yamaguchi equation [30, 31]:

$$J = -\frac{E_{\mathrm{HS}} - E_{\mathrm{BS}}}{\langle\hat{S}^2\rangle_{\mathrm{HS}} - \langle\hat{S}^2\rangle_{\mathrm{BS}}}. \tag{2}$$

The advantage of the Yamaguchi approach consists in retaining its validity over the whole range of coupling strengths. To visualize the interacting non-orthogonal magnetic orbitals, which were used for revealing the spin coupling exchange pathways, the broken-symmetry spin-unrestricted solutions after the corresponding orbital transformation [32] were employed.

3 Results and Discussion

3.1 Mononuclear Surface Vanadyl Complexes

The optimized geometry of the vanadyl VO^{2+} unit hosted in the **5T** site is presented in Fig. 1a along with the selected bond distances. The [VO]-**5T** model of the isolated monomer shows tetrahedral structure around vanadium with the V=O moiety linked to two siloxy ($\equiv$Si–O^-) and one silanol (Si–OH) ligands, mimicking the functional groups of the surface. The vanadyl V=O bond length is equal to 1.618 Å with the Mayer bond order equal to b.o. = 2.02. The bond lengths between vanadium(IV) and siloxy ligands are equal to 1.848 Å, while for the silanol this distance is longer and equals 2.082 Å. The bonds formed with two siloxy ligands are rather strong and exhibit bond orders of b.o. = 0.86. The angles between the V=O bond and the bonds formed with the surface ligands are found to be $\angle$O=V–O_{siloxy} = 113° and $\angle$O=V–$O_{silanol}$ = 105°, and are close to the value characteristic of the tetrahedron.

From the magnetic point of view, the [VO]-**5T** complex is a classic $3d^1$ paramagnet with the spin density (Fig. 1b) being predominantly confined to the metal center ($\rho_V = 1.07$) and only slightly shifted toward the oxo moiety ($\rho_O = -0.12$) due to the spin polarization effect. The metal spin density is largely associated with the nonbonding $3d_{xy}$ ground state (74%). Such a unit, bearing the dominant part of the spin density and being responsible for the magnetic properties of the system as a whole, was termed a magnetophore [33].

3.1.1 Spin-Hamiltonian Parameters

The quality of the [VO]-**5T** molecular model was examined by computation of the **g** and **A** tensors and comparison with the corresponding EPR parameters, extracted from the computer simulations of the experimental spectra. To ascertain the optimal combination of the exchange–correlation functional, basis set, and approximation of the relativistic effects, the benchmark calculations against the measured spin-Hamiltonian parameters of the akin $VO(acac)_2$ molecular complex [34] were carried

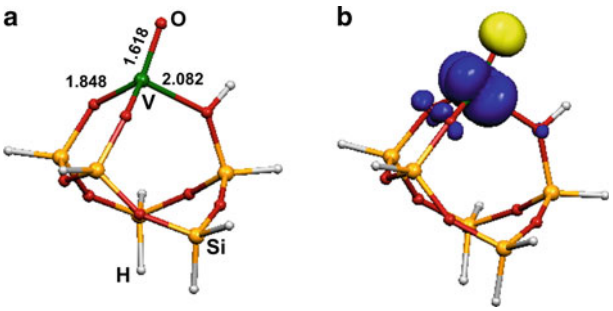

Fig. 1 **a** Optimized geometry and **b** corresponding spin density contour (*blue* positive values, *yellow* negative values, cutoff equal to 0.005) of the [VO]-**5T** surface complex. Selected bond lengths are given in angstroms (color figure online)

out. The results are collected in Table 1. On account of the very good agreement between experiment and theory obtained for the test $VO(acac)_2$ complex, the following calculation scheme was adopted for further modeling: B3LYP* functional (with the exact Hartree–Fock exchange increased from 0.20 to 0.35), TZV basis set for O, C, and H atoms, and CP(PPP) basis set [35] for vanadium, SOMF approximation of relativistic effects.

The calculated spin-Hamiltonian parameters for the [VO]-**5T** complex are typical of mono-oxovanadium(IV) complexes trapped on oxide surfaces and, as expected, are similar to those found for the analogous molecular systems with the common V=O magnetophore [3, 10, 13, 15, 16, 34]. As can be seen in Table 1, the calculated **g** tensor agrees well with the experimental values. Only in the case of the g_{zz} component, the obtained shift is noticeably exaggerated. However, in accordance with the experimental data, the g-shift of this component is bigger for the surface vanadyl complex in comparison with $VO(acac)_2$; thus, the general tendency is predicted acceptably. Similarly, for the calculated hyperfine parameters the agreement with the experimental data is quite satisfactory, proving a correct composition of the spin density repartition within the investigated complex. An apparent uniform shift to lower values of all hyperfine components, with respect to the experimental data, can be accounted for by a slight underestimation of the a_{iso} value. Taking into account the atomic value of the Fermi contact for the ^{51}V nucleus, this disagreement corresponds to 7–12% error in the spin density calculation.

3.2 Surface Dinuclear Vanadyl Complex

The optimized geometry of the dimer complex [VO–O–VO]-**6T** is shown in Fig. 2a, along with the values of some selected geometry parameters. The coordination stereochemistry of the dimer entity can be analyzed in terms of two tetrahedral vanadyl VO^{2+} subunits, sharing one common corner that forms the μ-oxo bridge. Each of the vanadium subunits is linked to the surface via one silanol and one siloxy groups, which are modeled with the **6T** cluster. The oxygen–vanadium bond lengths of both terminal vanadyl groups ($d_{V=O} = 1.614$ Å and b.o. = 2.06) are slightly shorter than those in the case of the monomer species. The dimer tends to be highly

Table 1 Calculated and experimental **g** and **A** tensors of the molecular $VO(acac)_2$ complex and the isolated surface vanadyl [VO]-**5T** species

Structure	g_{xx}	g_{yy}	g_{zz}	$\lvert A_{xx}\rvert$ (MHz)	$\lvert A_{yy}\rvert$ (MHz)	$\lvert A_{zz}\rvert$ (MHz)	Reference
Calculated							
$VO(acac)_2$	1.977	1.980	1.953	177	154	504	this work
[VO]-**5T**	1.982	1.989	1.890	167	156	514	this work
Experimental							
$VO(acac)_2$	1.975	1.979	1.947	180	168	502	[34]
$V^{IV}O$-silica	1.970	1.970	1.927	204	204	545	[15]
	1.976	1.976	1.930	187	187	530	[10]

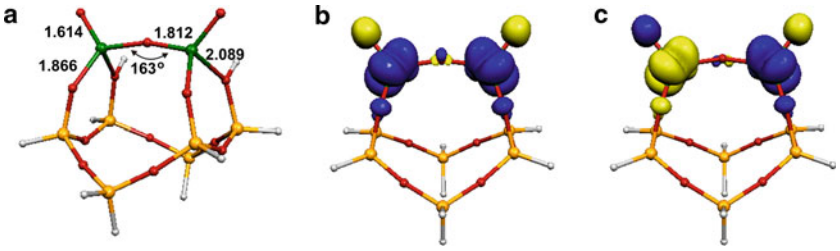

Fig. 2 Optimized geometry of the [VO–O–VO]-**6T** complex (**a**) along with the spin density contours (cutoff equal to 0.005) of the high-spin state (**b**) and the broken-symmetry state (**c**). Positive areas of the spin density are indicated in *blue*, negative in *yellow*, whereas the selected bond lengths are given in angstroms, and angles are given in degrees (color figure online)

symmetric since the distances between the bridging oxygen and both vanadium(IV) cores are identical and equal to 1.812 Å (b.o. = 0.86). Furthermore, the interaction of the dimer species with the surface ligands is apparently weaker than in the case of the monomer. It is clearly reflected in the values of the bond distances and bond orders obtained for vanadium–siloxy ligand ($d_{\mathrm{V-siloxy}} = 1.866$ Å, b.o. = 0.72) and vanadium–silanol ligand ($d_{\mathrm{V-silanol}} = 2.089$ Å, b.o. = 0.23). The oxo bridge assumes a bent configuration with the angle of $\angle$V–O–V = 163°, whereas the angle between the V=O moiety and the bridge is equal to $\angle$O=V–O = 120°.

3.2.1 Broken Symmetry Calculations

In the case of two interacting subsystems with spatially separated spins of $S_1 = ½$ and $S_2 = ½$, parallel and antiparallel coupling of the individual spins yields the effective $S = 1$ for the HS and $S = 0$ for the BS state. The relative energy levels of the spin states are gauged by the exchange coupling constant J, according to the equation:

$$E(S) = -JS(S+1), \tag{3}$$

where J can be calculated using Eq. (2).

The computed spin densities of the HS and BS states are shown in Fig. 2b and c, respectively. The contours indicate a strong confinement of the spin density within the divanadium(IV) species. For the HS state, the site spin densities account for 59% $3d_z^2$ and 22% $3d_{xy}$ for each vanadium site. In comparison with the monomeric complex, the spin density of the dimeric species exhibit clearly different composition, which results from the more distorted fourfold coordination around the vanadium centers.

The broken symmetry solution displays regions of the positive and negative spin densities (Fig. 2c), with the integral over the whole space being averaged to zero. This is a qualitatively wrong characteristic (which is a well-known feature of the broken symmetry solution [32]) since the correct singlet wavefunctions exhibit zero spin density at each point in the space. The calculated atomic spin populations for the vanadyl units are equal to $\rho(\mathrm{V}^{(1)}) = 1.09$, $\rho(\mathrm{O}^{(1)}_{\mathrm{oxo}}) = -0.15$, $\rho(\mathrm{V}^{(2)}) = -1.09$, $\rho(\mathrm{O}^{(2)}_{\mathrm{oxo}}) = 0.15$. In this case, the entire $(\mathrm{VO–O–VO})^{2+}$ complex plays a role of the

magnetophore. The broken symmetry calculations gave exchange coupling constant $J = -26\ \mathrm{cm}^{-1}$. Since the superexchange depends on the orientation of the magnetic orbitals with respect to each other, one may expect a distinct structure sensitivity of the calculated J values to the angle formed by the V–O–V bridge. Preliminary assessment showed that for the generic structure of the oxo-bridged dimers supported on silica depicted in Fig. 2, the J values are in the range of $-21 \pm 5\ \mathrm{cm}^{-1}$ for the V–O–V angle varying from 100° to 160°.

The antiferromagnetic coupling indicates that the BS solution is lower in energy than the HS state. Similar result has been obtained for the molecular divanadium(IV) μ-hydroxo complexes [16]. As a consequence, the surface dimers with the antiferromagnetic $(VO–O–VO)^{2+}$ bridges are EPR silent, as has been experimentally deduced from the observed decrease of the EPR signal intensity with the increasing total vanadium loading [36]. Indeed, according to Eq. (3), the calculated J value corresponds to the energy separation between the ground singlet and the excited triplet equal to $\Delta E = -2J = 52\ \mathrm{cm}^{-1}$. At 77 K, a typical temperature of EPR measurements, the thermal energy equals to $53.5\ \mathrm{cm}^{-1}$. In such conditions, spin population of the excited triplet is appreciable, but due to expected fast relaxation the EPR signal would be broadened beyond the detection limit. Although lowering the temperature to 4 K slows down the relaxation, it leads at the same time to a deep depopulation of the magnetically active triplet state, making detection of the EPR signal even more difficult. At the same time no vanadium in its oxidation state V(III) was detected [37], which could also account for the observed decrease of the intensity of X-band EPR spectra.

For a better understanding of the electronic structure of the exchange-coupled surface divanadium(IV) species, contours of the corresponding orbitals were calculated and collated in Fig. 3. These orbitals were calculated based on the transformation such that for the transformed spin-unrestricted orbitals each occupied spin-up orbital has a spatial overlap unequal to zero with at most one spin-down orbital. This procedure is known as the corresponding orbital transformation [32]. In general, the corresponding orbital transformation leads to three types of solutions. The first one, involving essentially doubly occupied $\alpha\beta$ spin pairs, exhibits spatial overlap close to unity. The possible slight deviation from this ideal value can be caused by spin polarization. These are the $119\alpha\beta$ and $120\alpha\beta$ orbital pairs, and all other orbitals lower in energy not shown in Fig. 3. The most interesting type of the corresponding orbitals is represented by $|S_{HS} - S_{BS}|$ non-orthogonal magnetic pairs, characterized with small but nonzero overlap. For the [VO–O–VO]-**6T** structure, there are two such orbitals, namely 121α and 121β (Fig. 3). The last type of the corresponding orbitals is given by the unmatched spin-up orbitals, representing the virtual states.

The corresponding orbitals of two magnetic electrons give rise to one exchange pathway with reasonable overlap ($S = 0.11$). This pathway, shown in Fig. 3, can be described as a symmetric π–π overlap caused by the interaction between the in-plane p-orbitals of the oxo bridge and the $3d_{xy}$ vanadium orbitals. Such a pathway indicates that the antiferromagnetic coupling is mediated by superexchange via the μ-oxo bridge.

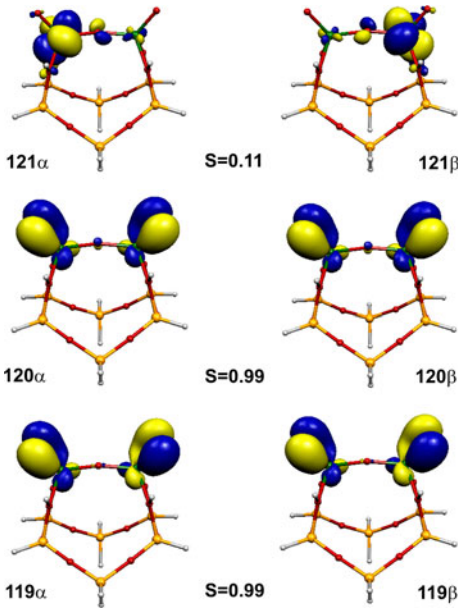

Fig. 3 Corresponding magnetic orbitals calculated for the broken-symmetry state of the [VO–O–VO]-**6T** surface complex in spin-unrestricted representation. *S* denotes the calculated values of the overlap for the appropriate orbital pairs

4 Conclusions

Two types of the vanadium(IV) entities, present on the reduced VO_x/silica surfaces, have been characterized theoretically and their magnetic structure and spin-Hamiltonian parameters have been accounted for by the relativistic DFT calculations. The isolated tetragonal vanadium(IV) complexes are strongly bound to the silica surface via two siloxy and one silanol ligands, and are characterized by the typical **g** and **A** parameters characteristic of the mono-oxovanadium(IV) magnetophore. The dimer entities composed of the μ-oxo-divanadium(IV) cores are attached to the silica support by involvement of the siloxy and silanol surface functional groups. DFT broken symmetry calculations for the dimer surface species show antiferromagnetic coupling between the mono-oxovanadium(IV) subunits. The antiferromagnetic interaction is mediated by the superexchange pathway via the μ-oxo bridge, as revealed by the contours of the corresponding orbitals.

Acknowledgments Financial support by the Ministry of Science and Higher Education (MNiSW) of Poland, Grant No. N N204 239334, is acknowledged. The calculations were carried out with the computer facilities of CYFRONET-AGH.

References

1. Z. Sojka, Catal. Rev. Sci. Eng. **37**, 461 (1995)
2. T. Spałek, P. Pietrzyk, Z. Sojka, J. Chem. Inf. Model. **45**, 18 (2005)
3. P. Pietrzyk, Z. Sojka, S. Dźwigaj, M. Che, J. Am. Chem. Soc. **129**, 14174 (2007)
4. P. Pietrzyk, M. Srebro, M. Radoń, Z. Sojka, A. Michalak, J. Phys. Chem. A (2011) doi:10.1021/jp109524t
5. P. Pietrzyk, K. Podolska, Z. Sojka, Chem. Eur. J. **15**, 11802 (2009)
6. Y.-M. Liu, W.-L. Feng, T.-C. Li, H.-Y. He, W.-L. Dai, W. Huang, Y. Cao, K.-N. Fan, J. Catal. **239**, 125 (2006)
7. V. Fornés, C. López, H.H. López, A. Martínez, Appl. Catal. A: Gen. **249**, 345 (2003)
8. B. Kartheuser, B.K. Hodnett, J. Chem. Soc., Chem. Commun. **13**, 1093 (1993)
9. C. Hess, Chem. Phys. Chem. **10**, 319 (2009)
10. M. Chiesa, V. Meynen, S. Van Doorslaer, P. Cool, E.F. Vansant, J. Am. Chem. Soc. **128**, 8955 (2006)
11. K.D. Chen, A.T. Bell, E. Iglesia, J. Catal. **209**, 35 (2002)
12. A. Brückner, Phys. Chem. Chem. Phys. **5**, 4461 (2003)
13. P. Pietrzyk, Z. Sojka, Stud. Surf. Sci. Catal. **158**, 617 (2005)
14. X. Rozanska, R. Fortrie, J. Sauer, J. Phys. Chem. C **111**, 6041 (2007)
15. V. Luca, D.J. MacLachlan, R. Bramley, Phys. Chem. Chem. Phys. **1**, 2597 (1999)
16. L. Zhang, Z. Chen, Chem. Phys. Lett. **345**, 353 (2001)
17. B.P. Feuston, S.H. Garofalini, J. Chem. Phys. **91**, 564 (1989)
18. N. Magg, B. Immaraporn, J.B. Giorgi, T. Schroeder, M. Bäumer, J. Döbler, Z. Wu, E. Kondratenko, M. Cherian, M. Baerns, P.C. Stair, J. Sauer, H.-J. Freund, J. Catal. **226**, 88 (2004)
19. P. Pietrzyk, J. Phys. Chem. B **109**, 10291 (2005)
20. M.J. Frisch, G.W. Trucks, H.B. Schlegel, G.E. Scuseria, M.A. Robb, J.R. Cheeseman, J.A. Montgomery Jr., T. Vreven, K.N. Kudin, J.C. Burant, J.M. Millam, S.S. Iyengar, J. Tomasi, V. Barone, B. Mennucci, M. Cossi, G. Scalmani, N. Rega, G.A. Petersson, H. Nakatsuji, M. Hada, M. Ehara, K. Toyota, R. Fukuda, J. Hasegawa, M. Ishida, T. Nakajima, Y. Honda, O. Kitao, H. Nakai, M. Klene, X. Li, J.E. Knox, H.P. Hratchian, J.B. Cross, C. Adamo, J. Jaramillo, R. Gomperts, R.E. Stratmann, O. Yazyev, A.J. Austin, R. Cammi, C. Pomelli, J.W. Ochterski, P.Y. Ayala, K. Morokuma, G.A. Voth, P. Salvador, J.J. Dannenberg, V.G. Zakrzewski, S. Dapprich, A.D. Daniels, M.C. Strain, O. Farkas, D.K. Malick, A.D. Rabuck, K. Raghavachari, J.B. Foresman, J.V. Ortiz, Q. Cui, A.G. Baboul, S. Clifford, J. Cioslowski, B.B. Stefanov, G. Liu, A. Liashenko, P. Piskorz, I. Komaromi, R.L. Martin, D.J. Fox, T. Keith, M.A. Al-Laham, C.Y. Peng, A. Nanayakkara, M. Challacombe, P.M.W. Gill, B. Johnson, W. Chen, M.W. Wong, C. Gonzalez, J.A. Pople, *Gaussian 03*, Revision E.01, Gaussian, Inc., Wallingford CT, (2004)
21. P.J. Stephens, F.J. Devlin, C.F. Chabalowski, M.J. Frisch, J. Phys. Chem. **98**, 11623 (1994)
22. R.H. Hertwig, W. Koch, Chem. Phys. Lett. **268**, 345 (1997)
23. A. Schäfer, C. Huber, R. Ahlrichs, J. Chem. Phys. **100**, 5829 (1994)
24. B. H. Schlegel, in *Ab Initio Methods in Quantum Chemistry-I*, ed. by K. P. Lawley, (Wiley, New York, 1987)
25. F. Neese, ORCA—An Ab Initio, DFT and Semiempirical Electronic Structure Package, version 2.6-04.2007 (Universität Bonn, Bonn, Germany, 2007)
26. F. Neese, J. Chem. Phys. **115**, 11080 (2001)
27. F. Neese, J. Chem. Phys. **118**, 3939 (2003)
28. L. Noodleman, J. Chem. Phys. **74**, 5737 (1981)
29. L. Noodleman, E.J. Baerends, J. Am. Chem. Soc. **106**, 2316 (1984)
30. K. Yamaguchi, Y. Takahara, T. Fueno, in *Applied Quantum Chemistry*, ed. by V. H. Smith (Reidel, Dordrecht, 1986), p. 155
31. T. Soda, Y. Kitagawa, T. Onishi, Y. Takano, Y. Shigeta, H. Nagao, Y. Yoshioka, K. Yamaguchi, Chem. Phys. Lett. **319**, 223 (2000)
32. F. Neese, J. Phys. Chem. Solids **65**, 781 (2004)
33. P. Pietrzyk, Z. Sojka, J. Phys. Chem. A **109**, 10571 (2005)
34. V. Nagarajan, B. Müller, O. Storcheva, K. Köhler, A. Pöppl, Res. Chem. Intermed. **33**, 705 (2007)
35. F. Neese, Inorg. Chim. Acta **337C**, 181 (2002)
36. A. Adamski, T. Spałek, Z. Sojka, Res. Chem. Intermed. **29**, 793 (2003)
37. A. Dinse, A. Ozarowski, C. Hess, R. Schomäcker, K.-P. Dinse, J. Phys. Chem. C **112**, 17664 (2008)